Interleukin-6 mediates PSAT1 expression and serine metabolism in TSC2-deficient cells

Ji Wang[a,1,2], Harilaos Filippakis[a,1], Thomas Hougard[a], Heng Du[a], Chenyang Ye[b], Heng-Jia Liu[a], Long Zhang[a], Khadijah Hindi[a], Shefali Bagwe[a], Julie Nijmeh[a], John M. Asara[c], Wei Shi[d], Souheil El-Chemaly[a], Elizabeth P. Henske[a,3], and Hilaire C. Lam[a,3]

[a]Pulmonary and Critical Care Medicine, Brigham and Women's Hospital, Harvard Medical School, Boston, MA 02115; [b]The F.M. Kirby Neurobiology Center, Boston Children's Hospital, Department of Neurology, Harvard Medical School, Boston, MA 02115; [c]Division of Signal Transduction, Beth Israel Deaconess Medical Center and Department of Medicine, Harvard Medical School, Boston, MA 02215; and [d]Department of Surgery, Children's Hospital Los Angeles, Keck School of Medicine, University of Southern California, Los Angeles, CA 90027

Edited by John Blenis, Weill Cornell Medicine, New York, NY, and accepted by Editorial Board Member Tak W. Mak June 17, 2021 (received for review January 29, 2021)

Tuberous sclerosis complex (TSC) and lymphangioleiomyomatosis (LAM) are caused by aberrant mechanistic Target of Rapamycin Complex 1 (mTORC1) activation due to loss of either *TSC1* or *TSC2*. Cytokine profiling of TSC2-deficient LAM patient–derived cells revealed striking up-regulation of Interleukin-6 (IL-6). LAM patient plasma contained increased circulating IL-6 compared with healthy controls, and TSC2-deficient cells showed up-regulation of IL-6 transcription and secretion compared to wild-type cells. IL-6 blockade repressed the proliferation and migration of TSC2-deficient cells and reduced oxygen consumption and extracellular acidification. U-^{13}C glucose tracing revealed that IL-6 knockout reduced 3-phosphoserine and serine production in TSC2-deficient cells, implicating IL-6 in de novo serine metabolism. IL-6 knockout reduced expression of phosphoserine aminotransferase 1 (PSAT1), an essential enzyme in serine biosynthesis. Importantly, recombinant IL-6 treatment rescued PSAT1 expression in the TSC2-deficient, IL-6 knockout clones selectively and had no effect on wild-type cells. Treatment with anti–IL-6 (αIL-6) antibody similarly reduced cell proliferation and migration and reduced renal tumors in *Tsc2*$^{+/-}$ mice while reducing PSAT1 expression. These data reveal a mechanism through which IL-6 regulates serine biosynthesis, with potential relevance to the therapy of tumors with mTORC1 hyperactivity.

tuberous sclerosis complex | lymphangioleiomyomatosis | mTORC1 | interleukin 6 | phosphoserine aminotransferase 1 (PSAT1)

Tuberous sclerosis complex (TSC) is an autosomal dominant tumor suppressor syndrome that affects one in 10,000 infants (1–4). The majority of patients suffer from neurodevelopmental conditions including epilepsy, autism, and cognitive impairment. Neoplastic lesions in the brain, skin, heart, kidneys, and lungs are the primary causes of patient morbidity and mortality, particularly later in life (5, 6). Renal angiomyolipomas affect ∼70% of patients by 10 y of age (7). Lymphangioleiomyomatosis (LAM), characterized by pulmonary nodules and irreversible progressive cystic lung destruction, almost exclusively affects females with TSC and can also affect women with sporadic LAM (4, 8).

TSC is caused by inactivating mutations in *TSC1* or *TSC2*, resulting in aberrant activation of mechanistic Target of Rapamycin Complex 1 (mTORC1), a master regulator of cellular metabolism (9). Constitutive mTORC1 activation leads to extensive changes in signaling pathways and promotes lipid, nucleotide, and protein biosynthesis contributing to the dysregulated growth and proliferation of cells in patients with TSC (10, 11). mTORC1 can be directly targeted by the allosteric inhibitor rapamycin and related analogs, "rapalogs," as well as catalytic mTOR inhibitors. Since mTORC1 inhibition primarily exerts cytostatic effects (7, 12), identifying novel therapeutic targets that can yield more durable or cytotoxic clinical responses is a key focus of ongoing TSC research.

Interleukin-6 (IL-6) is a secreted cytokine and critical mediator of inflammation (13). IL-6 binds to either soluble or membrane bound IL-6 receptor α. The IL-6/IL-6Rα complex then interacts with gp130 to activate signaling via Janus Kinase/Signal Transducer and Activator of Transcription 3 (JAK/STAT3). STAT3 regulates the transcription of hundreds of genes including IL-6. This positive feedback loop has been previously shown to be an epigenetic mechanism of transformation downstream of transient Ras activation (14). STAT3 activation by mTORC1 is a well described feature of TSC lesions, along with an increase in IL-6 production (15–23).

In support of prior findings, we find that IL-6 is up-regulated in the plasma of patients with LAM and in preclinical models of TSC in a TSC2- and mTORC1-dependent manner. By inhibiting IL-6 both genetically and with neutralizing antibodies, we find that TSC2-deficient cells depend on IL-6 to support the cell-autonomous metabolic reprogramming necessary for proliferation and migration. In particular, we implicate IL-6 in the regulation of de novo serine synthesis in TSC2-deficient cells. The enzymatic reactions necessary for de novo serine metabolism produce serine as well as antioxidants and the tricarboxylic acid (TCA) cycle intermediate, α-ketoglutarate. Specifically, the first rate-limiting step is executed by phosphoglycerate dehydrogenase (PHGDH), which converts the glycolytic intermediate 3-phoshphogylcerate to 3-phosphohydroxypyruvate, regenerating

Significance

The tumor suppressor syndrome tuberous sclerosis complex (TSC) affects 1:10,000 live births. We discovered that the inflammatory cytokine Interleukin-6 (IL-6) promotes the proliferation and migration of TSC2-deficient cells in part through the regulation of PSAT1 and de novo serine biosynthesis. Importantly, IL-6 neutralizing antibody treatments reduced renal cyst and cystadenoma formation in Tsc2$^{+/-}$ mice. This study highlights a therapeutically targetable vulnerability of TSC, which may have broad clinical application to mTORC1-activated tumors.

Author contributions: J.W., H.F., H.-J.L., K.H., E.P.H., and H.C.L. designed research; J.W., H.F., T.H., C.Y., H.-J.L., L.Z., K.H., S.B., S.E.-C., and H.C.L. performed research; S.B., J.M.A., W.S., and S.E.-C. contributed new reagents/analytic tools; J.W., H.F., T.H., H.D., J.M.A., W.S., and H.C.L. analyzed data; and J.W., H.F., J.N., E.P.H., and H.C.L. wrote the paper.

The authors declare no competing interest.

This article is a PNAS Direct Submission. J.B. is a guest editor invited by the Editorial Board.

[1]J.W. and H.F. contributed equally to this work.

[2]Present address: Plastic and Reconstructive Surgery Center, Department of Plastic and Reconstructive Surgery, Zhejiang Provincial People's Hospital, Affiliated People's Hospital, Hangzhou Medical College, 310014 Hangzhou, Zhejiang, China.

[3]To whom correspondence may be addressed. Email: hclam@bwh.harvard.edu or ehenske@bwh.harvard.edu.

This article contains supporting information online at https://www.pnas.org/lookup/suppl/doi:10.1073/pnas.2101268118/-/DCSupplemental.

Published September 20, 2021.

NADH from NAD. The next step is mediated by phosphoserine aminotransferase 1 (PSAT1), which converts 3-phosphohydroxypyruvate to 3-phosphoserine by transferring the amino group from glutamate and producing the TCA cycle intermediate a-ketoglutarate. Finally, 3-phosphoserine is converted to serine by phosphoserine phosphatase (PSPH). Serine can also be generated from glycine via the reversible action of serine hydroxymethyltransferase (SHMT) enzymes. Recent reviews have highlighted the importance of de novo serine metabolism in cancer survival and progression (24, 25). Our data implicate IL-6 as a regulator of de novo serine metabolism in mTORC1 hyperactive cells, thereby promoting the tumorigenic potential of TSC2-deficient cells.

Results

IL-6 Is Up-regulated in LAM Patient Plasma and Preclinical LAM and TSC Models. Previous studies have shown that TSC2-deficient cells have a unique secretome, which may support the proliferation and metastatic potential of TSC tumors and LAM nodules by both cell-autonomous and paracrine effects (21–23, 26). We performed a cytokine array using the TSC2-deficient 621-101 cell

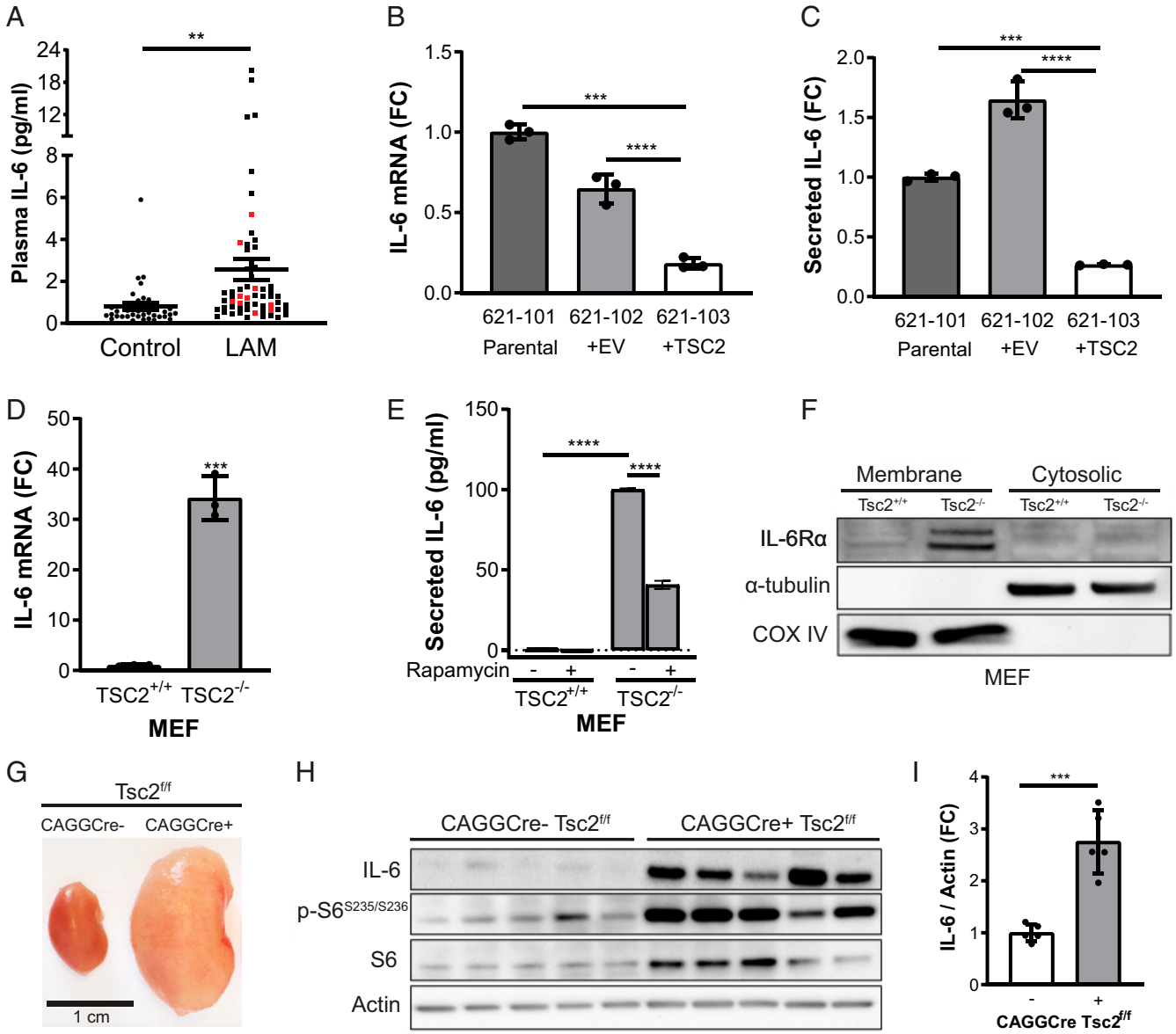

Fig. 1. IL-6 is overexpressed in TSC2-deficient cells and tissues. (*A*) IL-6 was increased in the plasma of LAM patients (total $n = 60$, black dots: sporadic LAM, $n = 50$; red dots: TSC-LAM, $n = 10$) compared to healthy controls ($n = 38$). The data are presented as the mean ± SEM. (*B*) IL-6 mRNA expression by qRT-PCR and (*C*) secreted IL-6 measured by ELISA are increased in TSC2-deficient human angiomyolipoma parental cells (621-101) and cells expressing empty vector (621-102) compared to cells with TSC2 addback (621-103). (*D*) qRT-PCR of IL-6 mRNA expression showing a 30-fold increase in $Tsc2^{-/-}$ MEFs compared to $Tsc2^{+/+}$ MEFs. (*E*) Rapamycin treatment decreases secreted IL-6 in TSC2-deficient MEFs as measured by ELISA (rapamycin; 20 nM, 24 h). (*F*) Western blot of membrane and cytosolic protein fractions of TSC2-deficient and wild-type MEFs. IL-6Rα is highly expressed in TSC2-deficient MEFs compared to TSC2-expressing MEFs. Cells were cultured in serum-free DMEM for 24 h before harvesting. α-tubulin used as a cytosolic fraction marker and COX IV as a membrane fraction marker. (*G*) Representative kidneys of *CAGGCre-ER*$^{TM+/-}$*; Tsc2*$^{f/f}$ and *CAGGCre-ER*$^{TM-/-}$*; Tsc2*$^{f/f}$ mice. (*H*) Western blot of *CAGGCre-ER*$^{TM+/-}$*; Tsc2*$^{f/f}$ and *CAGGCre-ER*$^{TM-/-}$*; Tsc2*$^{f/f}$ kidneys showing increased IL-6 expression upon TSC2 loss. (*I*) Densitometry of IL-6 protein levels normalized to actin in *CAGGCre-ER*$^{TM+/-}$*; Tsc2*$^{f/f}$ and *CAGGCre-ER*$^{TM-/-}$*; Tsc2*$^{f/f}$ kidney lysates shown in *H*. Data are presented as the mean ± SD of three independent experiments, unless indicated otherwise. One-way ANOVA, two-way ANOVA, or Student's *t* test were used for statistical analysis. $^{**}P < 0.01$, $^{***}P < 0.001$, $^{****}P < 0.0001$.

line derived from a human angiomyolipoma, in comparison to the human embryonic kidney cell line HEK293. The most robustly up-regulated cytokine in 621-101 cells was IL-6 (*SI Appendix*, Fig. S1 *A–D*), a factor previously reported in LAM in vivo models and patient-derived cells (21, 23). We discovered that IL-6 is also up-regulated in plasma from LAM patients compared to healthy controls (Fig. 1*A*).

We next confirmed that IL-6 expression is TSC2 dependent by comparing empty vector (621-102) or TSC2-addback cells (621-103) derived from the parental angiomyolipoma 621-101 cell

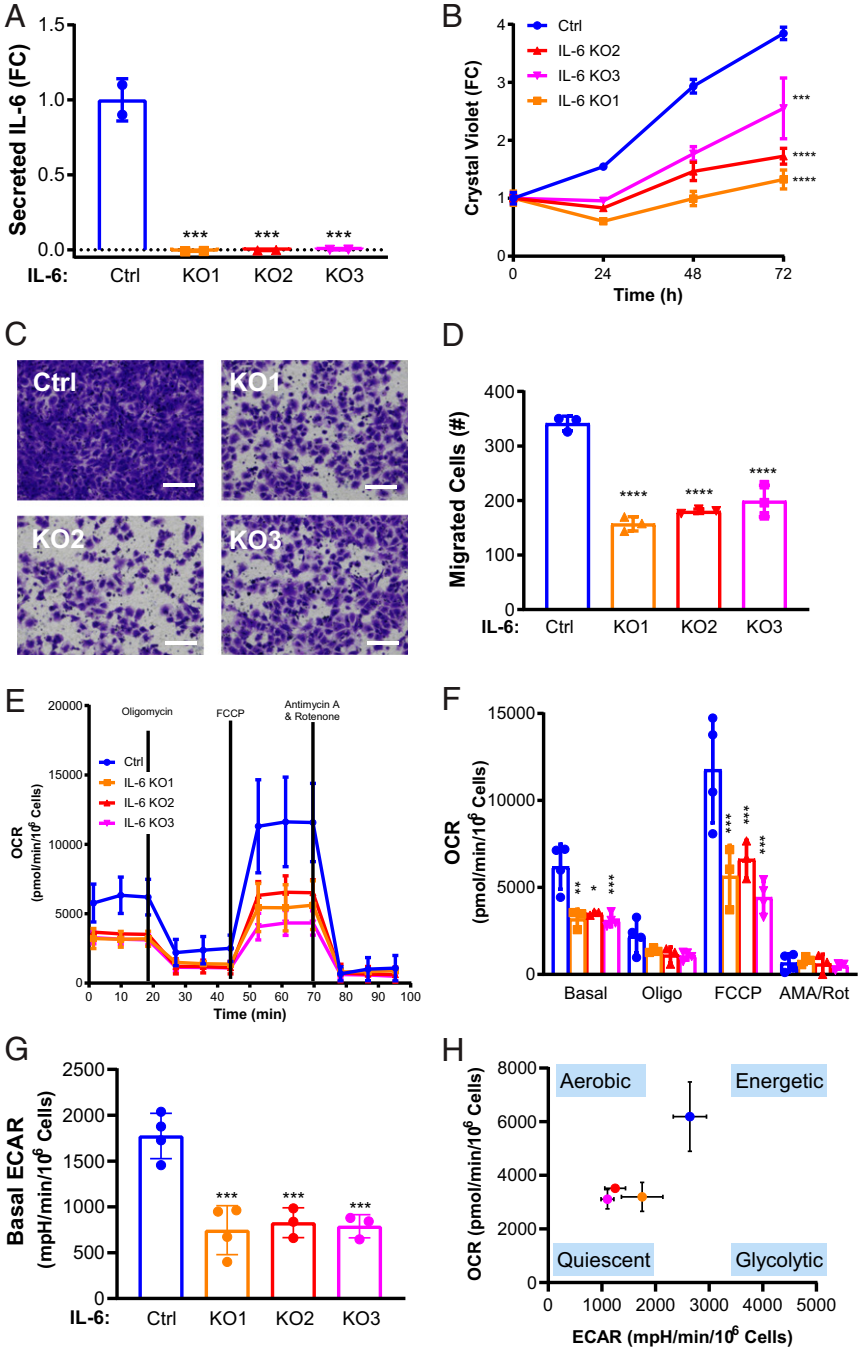

Fig. 2. IL-6 knockout suppresses proliferation and migration and induces a metabolic quiescent state in TSC2-deficient cells. (*A*) Secreted IL-6 is decreased in three IL-6 CRISPR/Cas9 clones compared to control, as measured by ELISA. (*B*) IL-6 knockout decreases the proliferation of TSC2-deficient MEFs compared to control as measured by crystal violet staining as a readout of cell density. (*C*) Representative images of (*D*) quantified cells migrated through transwells toward serum, which was decreased in IL-6 knockout; TSC2-deficient MEFs compared to TSC2-deficient control MEFs. (Scale bar, 100 μm.) (*E*) OCR is decreased in TSC2-deficient MEFs with IL-6 knockout compared to control cells. Data show measurements from the Seahorse extracellular flux analyzer using the MitoStress assay. (*F*) Summary and statistical analysis of OCR results. (*G*) Basal ECAR is decreased in TSC2-deficient MEFs with IL-6 knockout MEFs compared to control. mpH, milli-pH. (*H*) Energy map showing the global bioenergetic status of TSC2-deficient MEFs with IL-6 knockout compared to control. Data presented as the mean ± SD of three to four independent experiments. One-way ANOVA and Student's *t* test were used for statistical analysis. $*P < 0.05$, $**P < 0.01$, $***P < 0.001$, $****P < 0.0001$.

line. TSC2 reexpression significantly reduced *IL-6* messenger RNA (mRNA) expression and secretion of IL-6 (~70%, $P < 0.0001$) compared to the TSC2-deficient lines (Fig. 1 *B* and *C*). We next determined the expression and secretion of IL-6 in two additional pairs of TSC2-deficient and expressing cell lines: TTJ cells, derived from a renal tumor of a $Tsc2^{+/-}$ mouse, expressing either empty vector or reexpressing TSC2 and $Tsc2^{+/+}$ and $Tsc2^{-/-}$ mouse embryonic fibroblasts (MEFs) (27, 28). *IL-6* mRNA expression was up-regulated sevenfold in the TSC2-deficient TTJ cells relative to TSC2-expressing control cells ($P < 0.01$, *SI Appendix*, Fig. S1*E*) and by ~30-fold in the TSC2-deficient MEFs relative to TSC2-expressign MEFs ($P < 0.001$, Fig. 1*D*). Secretion of IL-6 was also increased in the TTJ cells ($P < 0.05$, *SI Appendix*, Fig. S1*F*) and TSC2-deficient MEFs ($P < 0.0001$, Fig. 1*E*). Rapamycin (20 nM, 24 h) partially reduced IL-6 secretion by ~50% ($P < 0.001$) in TSC2-deficient MEFs (Fig. 1*E*). Importantly, we found that IL-6 receptor α (IL-6Rα) is up-regulated in the membrane fraction of TSC2-deficient compared to TSC2-expressing MEFs, suggesting that IL-6 can act in an autocrine manner (Fig. 1*F*). IL-6 expression was also significantly elevated ~2.5-fold ($P < 0.001$) in kidney homogenates of *CAGGCre-ER*$^{TM+/-}$*; Tsc2*$^{f/f}$ mice, which are characterized by cystic kidney disease–driven mTORC1 hyperactivation, compared to *CAGGCre-ER*$^{TM-/-}$*; Tsc2*$^{f/f}$ control mice (Fig. 1 *G–I*) (29, 30).

In summary, these data show that IL-6 is up-regulated in patient plasma and consistently across numerous in vitro and in vivo models of TSC and LAM. Furthermore, IL-6 expression is both TSC2 and mTORC1 dependent. Finally, the increased expression of IL-6Rα on the TSC2-deficient cells suggests that IL-6 may be secreted and detected by TSC2-deficient cells, thereby exerting cell-autonomous effects.

IL-6 Knockout Suppresses Proliferation and Migration and Induces a Metabolic Quiescent State in TSC2-Deficient Cells. To investigate the dependance of TSC2-deficient cells on IL-6, we used CRISPR/Cas9 to knock out IL-6 from TSC2-deficient MEFs. We validated the knockout by measuring IL-6 secretion in three separate single cell clones generated from a single CRISPR/Cas9 guide (Fig. 2*A*). Genetic knockout of IL-6 decreased the proliferation of TSC2-deficient cells in serum-free conditions in comparison to IL-6–expressing TSC2-deficient cells (>30%, $P < 0.001$) as assessed by crystal violet staining as an indicator of cell density changes over 3 d (Fig. 2*B*). In order to maximize the differences between TSC2-deficient and wild-type control cells and to eliminate the possibility of the cells reacting to bovine IL-6 in the serum, we chose serum-free conditions for all subsequent experiments. Since metastasis is a key aspect of LAM pathogenesis, we also wanted to investigate the impact of IL-6 on the migration capacity of TSC2-deficient cells (31, 32). We discovered that IL-6 knockout also suppressed migration of TSC2-deficient cells through transwells toward a chemoattractant and in wound-healing assays compared to control cells (Fig. 2 *C* and *D* and *SI Appendix*, Fig. S2 *A* and *B*). Importantly, conditioned media from TSC2-deficient cells with intact IL-6 rescued proliferation of the IL-6 knockout cells (*SI Appendix*, Fig. S2*C*). Treatment with recombinant IL-6 (rIL-6) (200 pg/mL) rescued the proliferation and migration of the TSC2-deficient cells with IL-6 knockout (*SI Appendix*, Fig. S2 *D* and *E*)

To elucidate the mechanisms through which IL-6 knockout inhibits the proliferation of TSC2-deficient cells, we examined oxidative phosphorylation and glycolysis using the Seahorse XF Analyzer. The MitoStress Test Assay utilizes the effects of various mitochondrial targeted compounds on oxygen consumption rate (OCR) and extracellular acidification rate (ECAR) as a readout of the cellular potential for oxidative phosphorylation (OXPHOS) and aerobic glycolysis, respectively. Prior studies have shown that TSC2-deficient cells up-regulate glycolysis and OXPHOS to sustain the high bioenergetic and anabolic demands of mTORC1 hyperactivation (33–35). We found an overall decrease in OCR in the IL-6 knockout, TSC2-deficient cells compared to TSC2-deficient control cells expressing IL-6 (Fig. 2*E*). Statistical analysis of the OCR data demonstrated that both basal and maximal respiration (FCCP-induced) were significantly reduced ~50% ($P < 0.001$) in all three IL-6 knockout clones (Fig. 2*F*). We also found that IL-6 knockout suppressed aerobic glycolysis by ~50% ($P < 0.001$, Fig. 2*G*). The reduction in both OCR and ECAR suggests that IL-6 knockout shifts TSC2-deficient cells to a bioenergetic quiescent state (Fig. 2*H*). Acute treatment with recombinant IL-6 (200 pg/mL, 24 h) had no impact on the OCR or glycolytic profile of IL-6 KO cells (*SI Appendix*, Fig. S2 *F* and *G*).

Collectively, these data demonstrate that IL-6 knockout has a significant impact on proliferation, migration, and metabolism of TSC2-deficient cells, suggesting that IL-6 may be a previously unappreciated mediator of metabolic reprogramming in TSC.

IL-6 Promotes De Novo Serine Synthesis in TSC2-Deficient Cells. Since we observed an IL-6–dependent reduction in oxidative phosphorylation and glycolysis, we investigated the role of IL-6 in TSC2-deficient cell metabolism by performing targeted metabolomics, measuring ~270 unique metabolites by liquid chromatography/mass spectrometry (36). The IL-6 knockout clones showed a distinctive metabolic signature (*SI Appendix*, Fig. S3*A* and SI Table 1). There was some variability between the three clones, as expected from the process of single-cell cloning; however, principal component analysis confirmed that the clones were more similar to one another than the TSC2-deficient control cell line (*SI Appendix*, Fig. S3*B*).

We next performed metabolite set enrichment analysis using MetaboAnalyst software by curating a single list of consistently differentially regulated metabolites from pairwise comparisons of the control cells with each of the IL-6 knockout clones. The most significantly impacted pathway ($P < 0.0003$) with a false discovery rate less than 5% was glycine and serine metabolism (*SI Appendix*, Fig. S3*C*). Glycolytic intermediates can be diverted from the TCA cycle for utilization in de novo serine synthesis and the pentose phosphate pathway (PPP). In tumors, up-regulation of de novo serine metabolism and PPP supports nucleotide metabolism and redox homeostasis (37, 38). TSC2-deficient cells with IL-6 knockout have a >2-fold reduction in 3-phosphoserine ($P < 0.001$, *SI Appendix*, Fig. S4*A*) and a ~25% reduction in total serine levels ($P < 0.0001$, *SI Appendix*, Fig. S4*B*). Glycine was not measured in our samples, and cysteine was not changed by knocking out IL-6 (*SI Appendix*, Fig. S4*C*). We also discovered a ~40% reduction in ribose 5-phosphate, a PPP intermediate, and ~50% reduction in purines following IL-6 knockout in TSC2-deficient cells (*SI Appendix*, Fig. S4 *D* and *E*).

While early metabolites of the TCA cycle (citrate, aconitate, and isocitrate) were increased greater than twofold (*SI Appendix*, Fig. S4 *F–H*), metabolites downstream of α-ketoglutarate, which can be produced by glutaminolysis, were unaffected or decreased by IL-6 loss (*SI Appendix*, Fig. S4 *I–M*). One possible explanation for this result is that decreased flux of glycolytic intermediates into PPP and de novo serine synthesis following IL-6 knockout increases flux into the TCA cycle. These data suggest that IL-6 plays a significant role in the metabolism of TSC2-deficient cells, particularly glucose utilization.

To further investigate the impact of IL-6 on glucose metabolism, we used U-^{13}C glucose tracing and measured labeled metabolites after 0, 1, 3, and 24 h (39), focusing on the fractional enrichment of metabolites directly related to glucose metabolism (Fig. 3*A* and SI Table 2). All statistical analysis was performed at the final 24-h time point shown in the bar graphs below the time course data. The M+3 forms of serine (Fig. 3*B*) and 3-phosphoserine (Fig. 3*C*) were decreased in the cells with IL-6 knockout compared to controls with intact IL-6 by ~50% ($P < 0.0001$). Enrichment of M+3

phosphoglycerate was equal between the IL-6 knockout lines and TSC2-deficient controls, suggesting that IL-6 selectively effects shuttling of glycolytic intermediates into the de novo serine synthesis pathways (Fig. 3*D*). IL-6 knockout decreased glucose-derived M+2 α-ketoglutarate by ∼50% ($P < 0.001$, Fig. 3*E*) and increased glucose-derived M+2 glutamate by ∼10% ($P < 0.01$, Fig. 3*F*).

Glucose tracing data provide insights into the steady-state targeted metabolomics data, highlighting a significant reduction in the TCA cycle intermediate α-ketoglutarate derived from glucose. Furthermore, knocking out IL-6 in TSC2-deficient cells selectively suppressed glucose-derived intermediates from shuttling into de novo serine synthesis, thereby impacting the production of serine.

PSAT1 Rescues Proliferation of TSC2-Deficient Cells following IL-6 Knockout. To identify the potential molecular mechanisms through which IL-6 regulates de novo serine synthesis in TSC2-deficient cells, we measured the mRNA expression of the key

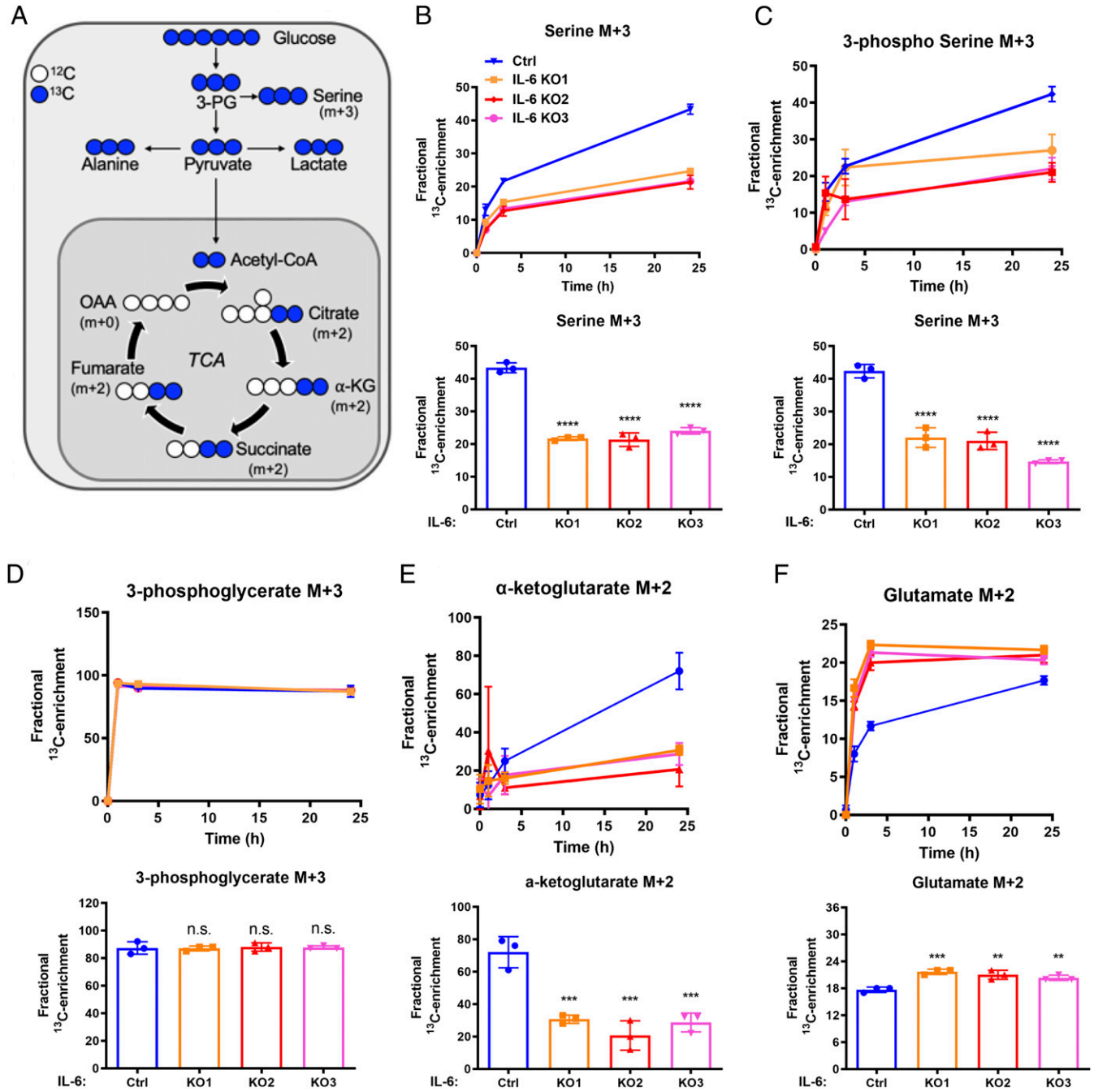

Fig. 3. IL-6 regulates de novo serine synthesis in TSC2-deficient cells. (*A*) Schematic of U-^{13}C-glucose metabolism. The incorporation of ^{13}C atoms from $^{13}C_6$-glucose into citrate, α-ketoglutarate (α-KG), succinate, fumarate, and oxaloacetate (OAA) are denoted as M + n, where n is the number of ^{13}C atoms. (*B–F*). Fractional enrichment of the M + 3 isotopologues of serine, 3-phosphoserine, and 3-phosphoglycerate or M + 2 isotopologues of α-KG and glutamate in TSC2-deficient MEFs with IL-6 knockout compared to TSC2-deficient controls (0, 1, 3, and 24 h after labeling; *Upper*). Bar graphs show statistical analysis at the 24-h time point (*Bottom*). Data presented as mean ± SD of three biological replicates. Statistical analysis performed by one-way ANOVA. $^{**}P < 0.01$, $^{***}P < 0.001$, $^{****}P < 0.0001$ or nonsignificant (n.s.) as compared to control.

metabolic enzymes of the pathway, *PHGDH*, *PSAT1*, and *PSPH* (Fig. 4 *A–D*). All three of the enzymes were significantly reduced at the mRNA level (>30%, $P < 0.01$) in the IL-6 knockout clones compared to the control TSC2-deficient cells.

We next confirmed the dependency of *PSAT1* on IL-6 signaling in the TSC2-deficient cells using short interfering RNA (siRNA) for IL-6Rα. A 90% reduction in IL-6Rα significantly reduced *PSAT1* expression ~20% ($P < 0.01$, *SI Appendix*, Fig. S5*A*). Interestingly, knocking down IL-6 ~80% with siRNA had no effect on PSAT1 expression (*SI Appendix*, Fig. S5*B*), suggesting that TSC2-deficient cells are responding at least in part to binding of extracellular IL-6 to the IL6-Rα in a cell-autonomous manner to regulate PSAT1 and de novo serine biosynthesis.

Importantly, treatment with rIL-6 rescued the expression of PSAT1 in the knockout clones, inducing PSAT1 expression >3-fold ($P < 0.0001$, Fig. 5*E*). Recombinant IL-6 had no effect on de novo serine synthesis enzymes in the TSC2 wild-type MEFs (*SI Appendix*, Fig. S5*C*). rIL-6 also induced a >1.5-fold increase in PHGDH, PSPH, and cytosolic SHMT1 but not mitochondrially localized SHMT2 (*SI Appendix*, Fig. S5 *D* and *E*). These data highlight the regulation of de novo serine synthesis by IL-6 selectively in TSC2-deficient cells. IL-6 knockout reduced PSAT1 protein expression >25%, while PHGDH and PSPH protein expression were unchanged compared to the control TSC2-deficient MEFs (Fig. 4 *F–I*).

In order to gain insights into the mechanisms by which IL-6 may regulate the enzymes of de novo serine synthesis, we performed additional knockdown experiments. Using STAT3 siRNA and inducible Raptor and Rictor knockout MEFs (40), we determined that PSAT1 is regulated in a STAT3-independent and mTORC1-dependent manner (*SI Appendix*, Fig. S6 *A–C*). These data are consistent with the finding that PSAT1 mRNA is increased ~3-fold in TSC2-deficient cells compared to wild-type control cells (*SI Appendix*, Fig. S6 *D* and *E*), as described in previous literature reports (41). In these prior publications, activating transcription factor 4 (ATF4) has been implicated in PSAT1 regulation downstream of mTORC1. We discovered a ~15% decrease in *ATF4* mRNA by IL-6 knockout ($P < 0.001$, *SI Appendix*, Fig. S6*F*).

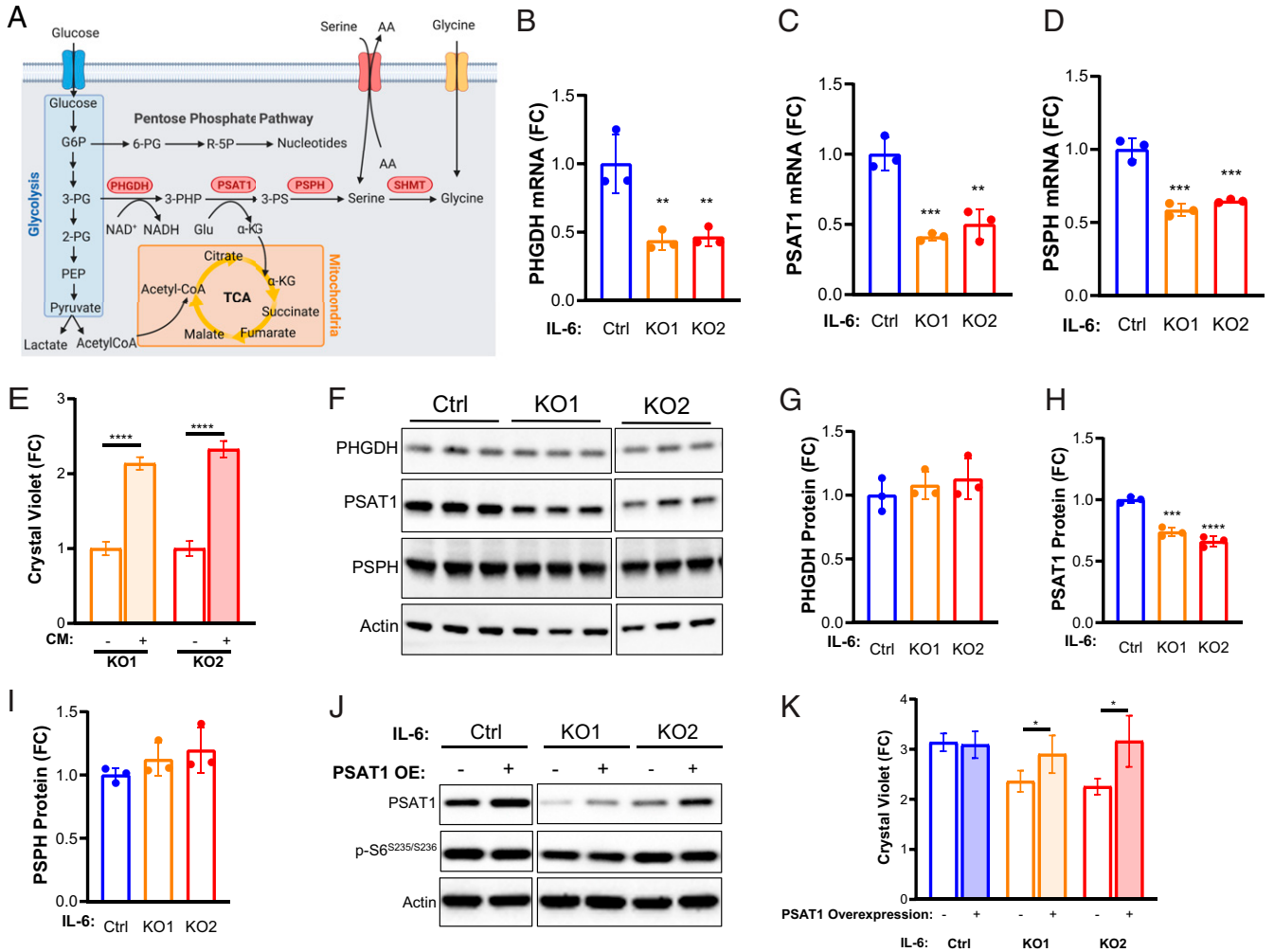

Fig. 4. PSAT1 rescues proliferation of TSC2-deficient, IL-6 knockout cells. (*A*) Diagram depicting interrelationships between glycolysis, the PPP, de novo serine biosynthesis, and the TCA. (*B–D*) PHGDH, PSAT1, and PSPH mRNA levels are decreased in TSC2-deficient, IL-6 knockout cells compared to TSC2-deficient control MEFs. (*E*) PSAT1 mRNA levels in IL-6 knockout, TSC2-deficient cells are rescued upon rIL-6 treatment (200 pg/mL; 24 h). (*F–I*) Western blot and densitometry showing expression of de novo serine biosynthesis enzymes and decreased PSAT1 expression in IL-6 knockout cells compared to control cells. Blots are from the same gel. Some lanes were cropped out for visualization purposes. (*J*) Western blot confirming PSAT1 overexpression in TSC2-deficient, IL-6 knockout cells and TSC2-deficient controls. Blots are from the same gel. (*K*) PSAT1 overexpression rescues proliferation of IL-6 knockout, TSC2-deficient cells (72 h; fold change relative to day 0, when the cells were washed and put into serum-free media). The data are presented as the mean ± SD of three independent experiments. One-way ANOVA was used for statistical analysis. *$P < 0.05$, **$P < 0.01$, ***$P < 0.001$, ****$P < 0.0001$ as compared to control.

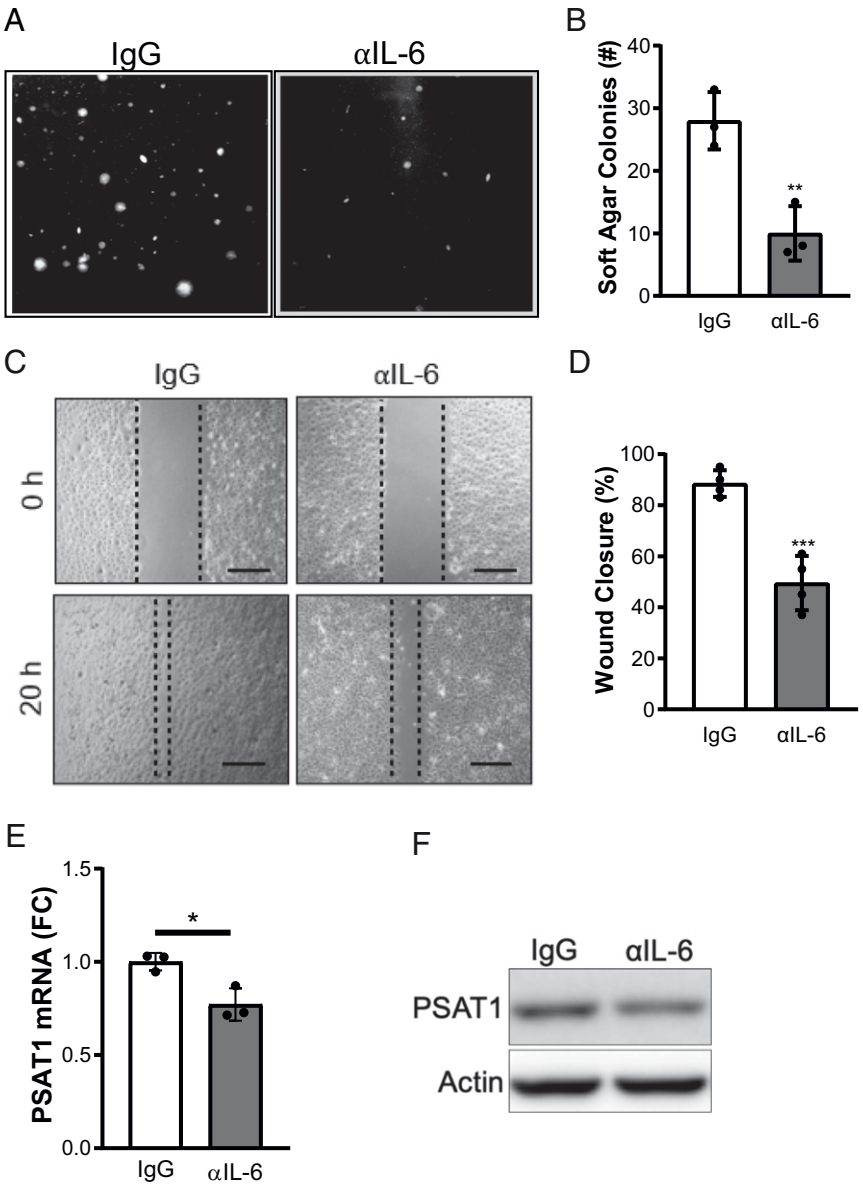

Fig. 5. αIL-6 antibody suppresses proliferation, migration, and PSAT1 expression in TSC2-deficient cells. (*A*) Representative images and (*B*) quantification of TSC2-deficient cell colonies grown for 14 d in soft agar and treated with αIL-6 or IgG control antibody (10 μg/mL) in serum-free DMEM. (Scale bar, 300 μm.) (*C*) Representative images and (*D*) quantification of wound-healing assay performed on TSC2-deficient cells treated with αIL-6 or IgG control antibody (10 μg/mL). αIL-6 treatment decreases wound closure of TSC2-deficient cells compared to IgG control antibody after 20 h (αIL-6; 10 μg/mL). Quantification of percent area filled between the two leading edges at 20 h compared to 0 h (0% filled). (Scale bar, 150 μm.) (*E*) PSAT1 mRNA and (*F*) PSAT1 protein are decreased by αIL-6 antibody (10 μg/mL; 48 h) in TSC2-deficient cells. Cells were grown in serum-free DMEM for the duration of the experiments. The data are presented as mean ± SD of three independent experiments. Student's *t* test was used for statistical analysis with $*P < 0.05$, $**P < 0.01$, $***P < 0.001$.

Interestingly, ATF4 protein expression and phosphorylation of S6 kinase were decreased in IL-6 knockout cells compared to IL-6–expressing cells (*SI Appendix*, Fig. S6*G*). Importantly, *ATF4* expression was induced ~2-fold ($P < 0.001$) by rIL-6 treatment in IL-6 knockout TSC2-deficient MEFs compared to TSC2 wild-type MEFs, in which *ATF4* expression was unchanged by rIL-6 (*SI Appendix*, Fig. S6 *H* and *I*). In order to determine the dependence of TSC2-deficient cells on PSAT1 downstream of IL-6, we overexpressed PSAT1 in the IL-6 knockout cells. Overexpression of PSAT1 was sufficient to rescue the proliferation of the IL-6 knockout cells and had no effect on the proliferation of the TSC2-deficient control cells (Fig. 4 *J* and *K*).

In summary, these data suggest that IL-6 promotes the proliferation of TSC2-deficient cells in a cell-autonomous manner via the up-regulation of PSAT1 and induction of de novo serine synthesis.

IL-6 Neutralizing Antibody Suppresses PSAT1 Expression, Proliferation, and Migration in TSC2-Deficient Cells. IL-6 and IL-6Rα neutralizing antibodies are approved by the Food and Drug Administration of the United States (FDA) for the treatment of various autoimmune diseases including rheumatoid arthritis (42). Therefore, we sought to determine whether anti–IL-6 (αIL-6) antibody treatment would impact the proliferation and migration of TSC2-deficient cells. We used p-STAT3^{Y705} expression as a surrogate marker of αIL-6 antibody activity (*SI Appendix*, Fig. S7 *A* and *B*). In order to more closely mimic the long-term consequences of αIL-6 antibody on the TSC2-deficient cells, we treated cells for 14 d and then

quantified colony formation in anchorage-independent soft agar conditions. αIL-6 antibody reduced colony formation by ∼60% ($P < 0.01$) compared to TSC2-deficent cells treated with control IgG antibody (Fig. 5 *A* and *B*). αIL-6 antibody also acutely reduced the migration of TSC2-deficient cells ∼40% compared to IgG antibody control ($P < 0.001$, Fig. 5 *C* and *D*).

We next wanted to determine if αIL-6 antibody treatment inhibited proliferation and migration effects by limiting de novo serine synthesis, as we observed in the IL-6 knockout cells. We discovered that αIL-6 significantly reduced PSAT1 expression and reduced the M+3 labeling of serine in the TSC2-deficient cells (Fig. 5 *E* and *F* and *SI Appendix*, Fig. S7*C* and SI Table 3). These data suggest that targeting IL-6 regulates PSAT1 expression and de novo serine synthesis in TSC2-deficient cells and may be a therapeutic approach for the treatment of TSC and LAM.

IL-6 Neutralizing Antibody Suppresses the Progression of Renal Tumors in TSC2$^{+/-}$ Mice. We next investigated the therapeutic impact of αIL-6 antibody in Tsc2$^{+/-}$ mice, a well-established preclinical model of TSC, which spontaneously develops renal cysts and cystadenomas by 6 mo of age (43). In the first set of experiments, we determined the therapeutic benefits of αIL-6 antibody as a single agent. The 8-mo-old Tsc2$^{+/-}$ mice were treated with αIL-6 antibody or control antibody (IgG) (200 μg, three times per week) for 1 mo (Fig. 6*A*) and harvested 24 to 48 h after the final injection. Kidneys were inspected macroscopically for gross cysts and tumor burden (Fig. 6*B*). αIL-6 antibody reduced both the gross and microscopic tumor burden ∼30% ($P < 0.05$) compared to the IgG-treated mice (Fig. 6 *B*–*D*). αIL-6 antibody also reduced the number of proliferating Ki67+ cells in the renal lesions (30%, $P < 0.01$, Fig. 6 *E* and *F*). Semiquantitative analysis of PSAT1 expression in renal lesions of the Tsc2$^{+/-}$ mice was performed by a blinded observer. Two out of three αIL-6 antibody–treated mice showed a decrease in the PSAT1 expression across >10 lesions per mouse (*SI Appendix*, Fig. S8 *A* and *B*).

mTORC1 inhibition with rapamycin and related rapalogs is currently approved for patients with LAM and TSC. In LAM patients, lung function decline stabilizes, and many brain lesions and renal tumors shrink on mTORC1 inhibitor treatment in

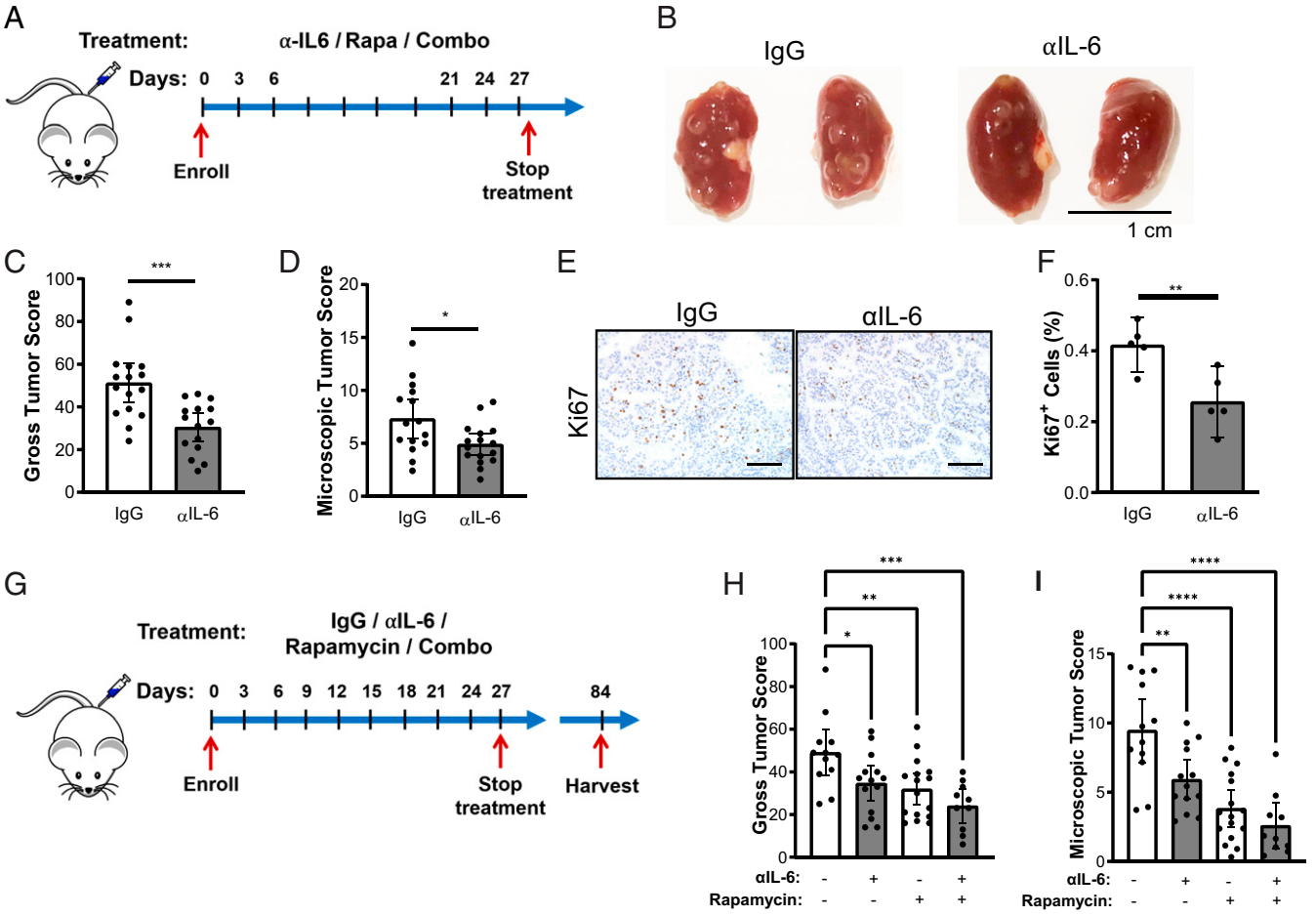

Fig. 6. αIL-6 antibody suppresses renal cystadenoma formation in *Tsc2*$^{+/-}$ mice. (*A*) Experimental design of αIL-6 antibody treatment. Tsc2$^{+/-}$ mice were injected intraperitoneally with IgG or αIL-6 antibody (200 μg/mouse, three times per week) for 1 mo and then harvested 24 to 48 h after the last injection. (*B*) Representative kidneys of *Tsc2*$^{+/-}$ mice injected intraperitoneally with IgG or αIL-6 antibody. (*C*) αIL-6 antibody decreased the gross tumor score and (*D*) microscopic tumor score of *Tsc2*$^{+/-}$ kidneys compared to IgG-treated kidneys. (*E*) Representative images of Ki67 staining in Tsc2$^{+/-}$ renal tumors and (*F*) quantification showing decreased proliferation in mice treated with αIL-6 antibody compared to IgG control mice. (Scale bar, 100 μm.) (*G*) Experimental design to determine the duration of therapeutic benefit following αIL-6, rapamycin, or combination treatments. Tsc2$^{+/-}$ mice were treated for 1 mo and then harvested 2 mo after the final injection. (*H*) Gross tumor score and (*I*) microscopic tumor score of kidneys from *Tsc2*$^{+/-}$ mice treated with IgG, αIL-6 (200 μg/mouse, three times/week), rapamycin (3 μg/kg three times/week), or the combination 2 mo after treatment cessation. Data are presented as the mean ± 95% CI; each dot represents one kidney. Statistical analysis was performed with Student's *t* test or one-way ANOVA. **P* < 0.05, ***P* < 0.01, ****P* < 0.001, *****P* < 0.0001.

patients with TSC (44, 45). However, disease burden rapidly rebounds after treatment cessation, necessitating novel therapeutic interventions. To determine the lasting effectiveness of αIL-6 antibody treatment compared to rapamycin or combination therapy (Fig. 6*G*), $Tsc2^{+/-}$ mice at 5 to 6 mo of age were randomly assigned to receive IgG, αIL-6 (200 μg, three times per week), rapamycin (3 mg/kg three times per week), or the combination (αIL-6 and rapamycin) for 1 mo. The mice were harvested 2 mo after the final treatment. All three treatment arms showed significant reduction in tumor burden compared to the IgG control mice (Fig. 6 *H* and *I*). The mean gross tumor score was reduced by 25% by αIL-6 antibody ($P < 0.01$), 30% by rapamycin ($P < 0.0001$), and 50% by the combination ($P < 0.0001$) compared to the IgG-treated controls. The mean microscopic tumor burden was reduced by 40% by αIL-6 antibody ($P < 0.01$), 60% by rapamycin ($P < 0.0001$), and 70% by the combination ($P < 0.0001$) compared to the IgG-treated controls.

In summary, we observed a significant benefit from αIL-6 antibody treatment and long-term benefits of 1-mo treatment with αIL-6 antibody. The combination of αIL-6 antibody and rapamycin appears to have an additive effect on tumorigenesis. These studies support the therapeutic potential of using clinically available approaches to target IL-6 in patients with TSC and LAM alone or in combination with mTORC1 inhibition.

Discussion

We have discovered that IL-6 cooperates with mTORC1 activation to support TSC-associated metabolic reprogramming. Using steady-state metabolomics in combination with U-^{13}C glucose tracing, we demonstrate that IL-6 plays a role in shunting glycolytic intermediates into de novo serine synthesis, a process which supports redox homeostasis and nucleotide metabolism in numerous tumors (41, 46–48). Our data suggest that IL-6 targeting has a significant impact on the metabolism and proliferation of TSC2-deficient cells. Interestingly, PSAT1 overexpression was sufficient to rescue the proliferation of the IL-6 knockout cells in the TSC2-deficient state, suggesting that regulation of serine metabolism is a key pathway downstream of IL-6. Serine, glycine, and one carbon metabolism fuels into numerous essential metabolic pathways (48, 49). Future studies will explore additional processes downstream of IL-6 and serine metabolism in the setting of mTORC1 hyperactivation. Notably, serine metabolism was shown to play a role in epigenetic processes following LKB1 loss and mTORC1 activation in KRAS-driven tumors (50). Serine availability is also important for the generation of certain lipid species known to be dysregulated in TSC2-deficient cells, suggesting another aspect of TSC biology that may be significantly impacted by inhibiting IL-6 (47, 51). These studies highlight the far-reaching effects on features of TSC pathogenesis, which may be mediated by IL-6 and serine metabolism.

IL-6 is a known autocrine, paracrine, and endocrine factor that has been implicated in the initiation, progression, and metastasis of numerous tumor types including skin, breast, lung, and kidney tumors (13, 52, 53). In this study, we focused on the cell-autonomous roles of IL-6 on the metabolism and tumorigenesis of TSC2-deficient cells. Interestingly, we discovered that circulating IL-6 levels are elevated in the serum of LAM patients and in TSC2-deficient human angiomyolipoma cells. Additionally, expression of IL-6Rα is elevated in TSC2-deficient cells, suggesting that IL-6 plays a role in a cell-autonomous manner. Interestingly, IL-6Rα can be shed into the extracellular milieu, allowing previously nonresponsive cells expressing the ubiquitous gp130 receptor to sense IL-6 (42, 54, 55). This mechanism of action highlights the exciting possibility that TSC2-deficient cells may also shed IL-6Rα to modulate the tumor microenvironment, exerting non–cell autonomous effects. Since recent studies have shown that TSC-associated pulmonary LAM and renal angiomyolipomas are responsive to immune checkpoint blockade (28, 56), the importance of the immune system in TSC and LAM disease progression has been well established. Importantly, IL-6–targeted therapies following mTORC1 activation caused by STK11/LKB1 loss in RAS-driven lung tumors decreased the immunosuppressive effects of tumor-associated neutrophils (57). Therefore, understanding the impact of IL-6–mediated signaling on the tumor microenvironment in TSC and LAM will be a critical next step for future studies.

IL-6 activates the pro-oncogenic transcription factor STAT3 via binding to IL-6Rα and gp130, leading to canonical JAK/STAT signaling. STAT3 activation is a well-described feature of TSC (15, 16, 19, 21, 23, 58, 59), including both brain and lung manifestations (16, 20). However, the mechanisms underlying this activation are not completely understood. We propose a model in which secreted IL-6 potentiates the STAT3 signal in TSC2-deficient cells. STAT3 is also directly activated by mTORC1-mediated phosphorylation on serine 727, a phosphorylation event required for maximal transcriptional activation (60). Together, these data support the activation of a STAT3/IL-6 positive feedback loop in TSC (61). Surprisingly, we discovered that IL-6 regulates de novo serine synthesis in a STAT3-independent manner in TSC2-deficient cells. Interestingly, the transcription factor, ATF4, known to regulate de novo serine synthesis enzymes (41, 62), was both mTORC1 dependent and regulated by IL-6. IL-6 activates additional protumorigenic pathways including RAS, phosphatidyl inositol 3-phosphate (PI3K-AKT), and Yes-associated protein/taffazin (YAP/TAZ) (13, 63–65). Furthermore, the IL-6 gene promoter contains an antioxidant response element and can be regulated by Nuclear Factor Erythroid 2 (NRF2) (66), which is up-regulated in TSC lesions (67) and has been previously implicated in regulating de novo serine synthesis in tumors (68). Finally, YAP/TAZ signaling has been shown to be up-regulated in TSC and plays a role in the regulation of transaminases in cancers (69, 70). Our data suggest that the regulation of de novo serine synthesis downstream of IL-6 may involve a complex interplay of transcription factors, many of which are implicated in TSC and LAM pathogenesis.

This project highlights potential therapeutic strategies for TSC and LAM. To assess the therapeutic potential of targeting IL-6 in TSC and LAM, we treated 8-mo-old $Tsc2^{+/-}$ mice that have established tumor burden with IL-6–neutralizing antibody (αIL-6 antibody). We demonstrate that αIL-6 antibody suppresses the formation of renal cysts and cystadenomas in $Tsc2^{+/-}$ mice. IL-6 targeted therapies are currently FDA approved for the treatment of rheumatoid arthritis and Castleman's disease (54, 55). Interestingly, we found only a partial reduction of IL-6 upon rapamycin treatment in vitro and an additive benefit of combining αIL-6 antibody with rapamycin in vivo. These data suggest that IL-6 pathway targeted therapies may work well in combination with mTORC1 inhibition, which is the standard of care for most patients with progressive TSC and LAM. Efforts are also underway to develop novel inhibitors of serine metabolism. These studies have shown that tumors must be in a serine-limited environment for maximal therapeutic potential. The brain is one organ system with low serine and glycine in which PHGDH inhibitors have shown therapeutic benefit in preclinical models (71), with possible implications for the various brain tumors that form in TSC. Finally, a serine/glycine limited diet has also been shown to improve the efficacy of these inhibitors in tumor models (72, 73).

In summary, we have uncovered a distinct IL-6–dependent metabolic signature, which plays an important role in supporting the proliferative and bioenergetic activity of TSC2-deficient cells. In particular, IL-6 appears to promote de novo serine biosynthesis and expression of the key intermediate enzyme, PSAT1. Targeting IL-6 with a neutralizing antibody exerts acute and durable therapeutic responses alone and in combination with rapamycin in vivo. Future studies may elucidate the molecular mechanisms by which IL-6 regulates de novo serine biosynthesis and the potential

therapeutic benefits of directly targeting de novo serine metabolism in TSC and LAM.

Materials and Methods

Cell Lines and Treatment. *Tsc2*$^{-/-}$*p53*$^{-/-}$ and *Tsc2*$^{+/+}$*p53*$^{-/-}$ MEFs were provided by David Kwiatkowski, Division of Pulmonary & Critical Care, Department of Medicine, Brigham and Women's Hospital, Boston, MA. The MEFs and stocks were prepared at passage 8. TTJ cells and 105 K were derived from a renal cystadenoma of a C57BL/6 *Tsc2*$^{+/-}$ mouse, with reexpressed Tsc2 or empty vector, as previously described (28). The 621-101 cells were isolated from a patient renal angiomyolipoma and immortalized with E6/E7, and the parental 621-101 cells were then use to reexpress Tsc2 (621-103) or empty vector (621-102), as previously described (74, 75). HEK293 cells were obtained from American Type Culture Collection (ATCC). Further details on cell lines used in this study can be found in *SI Appendix*.

Antibodies and Drugs. The following antibodies were used: TSC2 (Cell Signaling Technology, 4308S), S6 (2217S), pS6(2211L), IL-6 (Santa Cruz Biotechnology, sc-57315), STAT3 (9139S), pSTAT3 (9145S), PSAT1 (Protein Tech, No. 20180-1-AP), PHGDH (Protein Tech, No. 14719-1-AP), PSPH (Protein Tech, No. 14513-1-AP), β-actin (Sigma-Aldrich), K_i-67 (eBioscience, No. 14-5698-82). For immunohistochemistry, PSAT1 antibody (2102) was purchased from Origene. IL-6 neutralizing antibody and IgG control were purchased from Bioxcell (BE0046 and BE0088). Rapamycin and Torin1 were purchased from LC Laboratories. Recombinant mouse IL-6 (406-ML) was purchased from R&D.

Seahorse Assay. The MitoStress Test Assay and the Seahorse XFe24 analyzer were used. Cells were seeded into the XFe24 microplate and incubated for 24 h in 10% fetal bovine serum (FBS) Dulbecco's modified Eagle medium (DMEM). The next day, cells were washed with phosphate buffer saline (PBS) and cultured in FBS-free DMEM for 24 h. Compounds (final concentrations: 1 μM oligomycin, 1μM FCCP, 0.5 μM rotenone/antimycin A) were added to a prehydrated sensor cartridge. The sensor cartridge and XFe 24 microplate were placed in the XFe Analyzer. Results were normalized to cell number.

U-^{13}C Glucose Tracing. Cells (4×10^5) were seeded onto 60-mm plates in 10% FBS DMEM (Thermo Fisher Scientific, Gibco No. 11995123). The next day, the cells were washed with PBS and transferred to serum-free DMEM (Thermo Fisher Scientific, Gibco No. 11966025) supplemented with 4.5 g/L D-glucose. For U-^{13}C glucose tracing following αIL-6 antibody experiments, the cells also were washed with PBS and transferred to either αIL-6 antibody (10 μg/mL) or IgG (10 μg/mL) in serum-free DMEM (Thermo Fisher Scientific, Gibco No. 11966025) supplemented with 4.5 g/L D-glucose. At −24 h, −3 h, −1 h to harvest, the cells were washed with glucose-free and serum-free DMEM (Gibco No. 11966025) and then incubated in DMEM (No. 11966-025) supplemented with 4.5 g/L U-^{13}C Glucose (Sigma Aldrich) for 0 h, 1 h, 3 h, or 24 h. The cells were harvested and analyzed as described in *SI Appendix* (36, 39).

Human Plasma Specimens. Patient samples and healthy control samples were obtained through a Partner's Health Care Institutional Review Board approved protocol. Subjects gave consent to the clinical research team free of coercion, and samples were collected, deidentified, and coded. Plasma Interleukin-6 was measured by enzyme-linked immunosorbent assay (ELISA; R&D Quantikine Human IL-6 ELISA or High Sensitivity IL-6 ELISA).

Animal Studies. All animal studies were performed in accordance with institutional protocols approved by the Brigham and Women's Hospital Institutional Animal Care and Use Committee. For the cystic kidney model, we crossed the CAGGCRE-ER$^{TM+/-}$ (The Jackson Laboratory) to Tsc2 $^{flox/flox}$ (Michael Gambello, Department of Human Genetics, Emory University School of Medicine, Atlanta, GA). Recombination of Tsc2 was induced in 8- to 10-wk-old CAGGCRE-ER$^{TM+/-}$; Tsc2 $^{flox/flox}$ or control (CAGGCRE-ER$^{TM-/-}$; Tsc2 $^{flox/flox}$) mice with intraperitoneal tamoxifen (in corn oil) at a dose of 1 mg per day for five consecutive days. Kidneys were harvested at 5 mo of age. *Tsc2*$^{+/-}$ mice in the A/J background were generated in house as described previously (43, 76). Treatment schemes and quantitative analyses are described in detail in *SI Appendix*.

Statistical Analyses. Normally distributed data were analyzed for statistical significance with Student's unpaired *t* test and multiple comparisons were made with one-way and two-way ANOVAs with Bonferroni correction. In vivo data are presented as the mean ± 95% CI, and in vitro studies are presented as the mean ± SD. Analysis was performed using GraphPad Prism version 8; GraphPad Software, https://www.graphpad.com. Statistical significance was defined as $P < 0.05$.

Data Availability. All study data are included in the article and/or supporting information.

ACKNOWLEDGMENTS. This work was funded by the NIH (K01-DK116819 to H.C.L., R01HL146541 to W.S., and U01 HL131022-04 to E.P.H.,) and The Engles Family TSC/LAM Research Fund. The mass spectrometry work was partially funded by NIH Grants 5P01CA120964 (J.M.A.) and 5P30CA006516 (J.M.A.). We thank Dana-Farber/Harvard Cancer Center in Boston, MA, for the use of the Rodent Histopahtology Core, which provided tissue embedding and sectioning services. Dana-Farber/Harvard Cancer Center is supported in part by National Cancer Institute (NCI) Cancer Center Support Grant No. NIH 5P30 CA06516. We would also like to acknowledge Clemens K. Probst for technical assistance with experiments. Schematics were generated using https://Biorender.com. This work was performed in part to meet the requirements of the doctoral thesis of J.W. from Zhejiang University School of Medicine, Hangzhou, China.

1. J. P. Osborne, A. Fryer, D. Webb, Epidemiology of tuberous sclerosis. *Ann. N. Y. Acad. Sci.* **615**, 125–127 (1991).
2. F. J. O'Callaghan, A. W. Shiell, J. P. Osborne, C. N. Martyn, Prevalence of tuberous sclerosis estimated by capture-recapture analysis. *Lancet* **351**, 1490 (1998).
3. L. Hallett, T. Foster, Z. Liu, M. Blieden, J. Valentim, Burden of disease and unmet needs in tuberous sclerosis complex with neurological manifestations: Systematic review. *Curr. Med. Res. Opin.* **27**, 1571–1583 (2011).
4. E. P. Henske, S. Jóźwiak, J. C. Kingswood, J. R. Sampson, E. A. Thiele, Tuberous sclerosis complex. *Nat. Rev. Dis. Primers* **2**, 16035 (2016).
5. C. W. Shepherd, M. R. Gomez, J. T. Lie, C. S. Crowson, Causes of death in patients with tuberous sclerosis. *Mayo Clin. Proc.* **66**, 792–796 (1991).
6. H. Northrup, D. A. Krueger, International Tuberous Sclerosis Complex Consensus Group, Tuberous sclerosis complex diagnostic criteria update: Recommendations of the 2012 International Tuberous Sclerosis Complex Consensus Conference. *Pediatr. Neurol.* **49**, 243–254 (2013).
7. H. C. Lam, B. J. Siroky, E. P. Henske, Renal disease in tuberous sclerosis complex: Pathogenesis and therapy. *Nat. Rev. Nephrol.* **14**, 704–716 (2018).
8. K. H. Yu *et al.*, Data-driven analyses revealed the comorbidity landscape of tuberous sclerosis complex. *Neurology* **91**, 974–976 (2018).
9. A. Peron, K. S. Au, H. Northrup, Genetics, genomics, and genotype-phenotype correlations of TSC: Insights for clinical practice. *Am. J. Med. Genet. C. Semin. Med. Genet.* **178**, 281–290 (2018).
10. I. Ben-Sahra, B. D. Manning, mTORC1 signaling and the metabolic control of cell growth. *Curr. Opin. Cell Biol.* **45**, 72–82 (2017).
11. G. Y. Liu, D. M. Sabatini, mTOR at the nexus of nutrition, growth, ageing and disease. *Nat. Rev. Mol. Cell Biol.* **21**, 183–203 (2020).
12. L. J. McEneaney, A. R. Tee, Finding a cure for tuberous sclerosis complex: From genetics through to targeted drug therapies. *Adv. Genet.* **103**, 91–118 (2019).
13. K. Taniguchi, M. Karin, IL-6 and related cytokines as the critical lynchpins between inflammation and cancer. *Semin. Immunol.* **26**, 54–74 (2014).
14. D. Iliopoulos, H. A. Hirsch, K. Struhl, An epigenetic switch involving NF-kappaB, Lin28, Let-7 MicroRNA, and IL6 links inflammation to cell transformation. *Cell* **139**, 693–706 (2009).
15. K. M. Dodd, J. Yang, M. H. Shen, J. R. Sampson, A. R. Tee, mTORC1 drives HIF-1α and VEGF-A signalling via multiple mechanisms involving 4E-BP1, S6K1 and STAT3. *Oncogene* **34**, 2239–2250 (2015).
16. E. A. Goncharova *et al.*, Signal transducer and activator of transcription 3 is required for abnormal proliferation and survival of TSC2-deficient cells: Relevance to pulmonary lymphangioleiomyomatosis. *Mol. Pharmacol.* **76**, 766–777 (2009).
17. N. El-Hashemite, D. J. Kwiatkowski, Interferon-gamma-Jak-Stat signaling in pulmonary lymphangioleiomyomatosis and renal angiomyolipoma: A potential therapeutic target. *Am. J. Respir. Cell Mol. Biol.* **33**, 227–230 (2005).
18. J. A. Chan *et al.*, Pathogenesis of tuberous sclerosis subependymal giant cell astrocytomas: Biallelic inactivation of TSC1 or TSC2 leads to mTOR activation. *J. Neuropathol. Exp. Neurol.* **63**, 1236–1242 (2004).
19. N. El-Hashemite, H. Zhang, V. Walker, K. M. Hoffmeister, D. J. Kwiatkowski, Perturbed IFN-gamma-Jak-signal transducers and activators of transcription signaling in tuberous sclerosis mouse models: Synergistic effects of rapamycin-IFN-gamma treatment. *Cancer Res.* **64**, 3436–3443 (2004).
20. H. Onda *et al.*, Tsc2 null murine neuroepithelial cells are a model for human tuber giant cells, and show activation of an mTOR pathway. *Mol. Cell. Neurosci.* **21**, 561–574 (2002).
21. E. N. Atochina-Vasserman *et al.*, Surfactant dysfunction and lung inflammation in the female mouse model of lymphangioleiomyomatosis. *Am. J. Respir. Cell Mol. Biol.* **53**, 96–104 (2015).
22. E. A. Goncharova *et al.*, Prevention of alveolar destruction and airspace enlargement in a mouse model of pulmonary lymphangioleiomyomatosis (LAM). *Sci. Transl. Med.* **4**, 154ra134 (2012).
23. E. Lesma *et al.*, TSC2 epigenetic defect in primary LAM cells. Evidence of an anchorage-independent survival. *J. Cell. Mol. Med.* **18**, 766–779 (2014).

24. K. R. Mattaini, M. R. Sullivan, M. G. Vander Heiden, The importance of serine metabolism in cancer. *J. Cell Biol.* **214**, 249–257 (2016).
25. M. Reina-Campos, M. T. Diaz-Meco, J. Moscat, The complexity of the serine glycine one-carbon pathway in cancer. *J. Cell Biol.* **219**, e201907022 (2020).
26. M. Ding, R. K. Bruick, Y. Yu, Secreted IGFBP5 mediates mTORC1-dependent feedback inhibition of IGF-1 signalling. *Nat. Cell Biol.* **18**, 319–327 (2016).
27. H. Zhang *et al*., Loss of Tsc1/Tsc2 activates mTOR and disrupts PI3K-Akt signaling through downregulation of PDGFR. *J. Clin. Invest.* **112**, 1223–1233 (2003).
28. H. J. Liu *et al*., TSC2-deficient tumors have evidence of T cell exhaustion and respond to anti-PD-1/anti-CTLA-4 immunotherapy. *JCI Insight* **3**, e98674 (2018).
29. H. C. Lam *et al*., p62/SQSTM1 cooperates with hyperactive mTORC1 to regulate glutathione production, maintain mitochondrial integrity, and promote tumorigenesis. *Cancer Res.* **77**, 3255–3267 (2017).
30. N. Liang *et al*., Regulation of YAP by mTOR and autophagy reveals a therapeutic target of tuberous sclerosis complex. *J. Exp. Med.* **211**, 2249–2263 (2014).
31. F. X. McCormack, W. D. Travis, T. V. Colby, E. P. Henske, J. Moss, Lymphangioleiomyomatosis: Calling it what it is: A low-grade, destructive, metastasizing neoplasm. *Am. J. Respir. Crit. Care Med.* **186**, 1210–1212 (2012).
32. M. Guo *et al*., Single-cell transcriptomic analysis identifies a unique pulmonary lymphangioleiomyomatosis cell. *Am. J. Respir. Crit. Care Med.* **202**, 1373–1387 (2020).
33. H. C. Lam *et al*., Rapamycin-induced miR-21 promotes mitochondrial homeostasis and adaptation in mTORC1 activated cells. *Oncotarget* **8**, 64714–64727 (2017).
34. C. Priolo, E. P. Henske, Metabolic reprogramming in polycystic kidney disease. *Nat. Med.* **19**, 407–409 (2013).
35. E. E. Verwer *et al*., [^{18}F]Fluorocholine and [^{18}F]Fluoroacetate PET as imaging biomarkers to assess phosphatidylcholine and mitochondrial metabolism in preclinical models of TSC and LAM. *Clin. Cancer Res.* **24**, 5925–5938 (2018).
36. M. Yuan, S. B. Breitkopf, X. Yang, J. M. Asara, A positive/negative ion-switching, targeted mass spectrometry-based metabolomics platform for bodily fluids, cells, and fresh and fixed tissue. *Nat. Protoc.* **7**, 872–881 (2012).
37. M. A. Hawk, Z. T. Schafer, Mechanisms of redox metabolism and cancer cell survival during extracellular matrix detachment. *J. Biol. Chem.* **293**, 7531–7537 (2018).
38. R. Possemato *et al*., Functional genomics reveal that the serine synthesis pathway is essential in breast cancer. *Nature* **476**, 346–350 (2011).
39. M. Yuan *et al*., Ex vivo and in vivo stable isotope labelling of central carbon metabolism and related pathways with analysis by LC-MS/MS. *Nat. Protoc.* **14**, 313–330 (2019).
40. N. Cybulski, V. Zinzalla, M. N. Hall, Inducible raptor and rictor knockout mouse embryonic fibroblasts. *Methods Mol. Biol.* **821**, 267–278 (2012).
41. I. Ben-Sahra, G. Hoxhaj, S. J. H. Ricoult, J. M. Asara, B. D. Manning, mTORC1 induces purine synthesis through control of the mitochondrial tetrahydrofolate cycle. *Science* **351**, 728–733 (2016).
42. E. H. Choy *et al*., Translating IL-6 biology into effective treatments. *Nat. Rev. Rheumatol.* **16**, 335–345 (2020).
43. L. Lee *et al*., Efficacy of a rapamycin analog (CCI-779) and IFN-gamma in tuberous sclerosis mouse models. *Genes Chromosomes Cancer* **42**, 213–227 (2005).
44. C. D. Burger, Efficacy and safety of sirolimus in lymphangioleiomyomatosis. *N. Engl. J. Med.* **365**, 271–272 (2011).
45. J. J. Bissler *et al*., Sirolimus for angiomyolipoma in tuberous sclerosis complex or lymphangioleiomyomatosis. *N. Engl. J. Med.* **358**, 140–151 (2008).
46. I. Ben-Sahra, J. J. Howell, J. M. Asara, B. D. Manning, Stimulation of de novo pyrimidine synthesis by growth signaling through mTOR and S6K1. *Science* **339**, 1323–1328 (2013).
47. X. Gao *et al*., Serine availability influences mitochondrial dynamics and function through lipid metabolism. *Cell Rep.* **22**, 3507–3520 (2018).
48. M. Mehrmohamadi, X. Liu, A. A. Shestov, J. W. Locasale, Characterization of the usage of the serine metabolic network in human cancer. *Cell Rep.* **9**, 1507–1519 (2014).
49. M. A. Reid *et al*., Serine synthesis through PHGDH coordinates nucleotide levels by maintaining central carbon metabolism. *Nat. Commun.* **9**, 5442 (2018).
50. F. Kottakis *et al*., LKB1 loss links serine metabolism to DNA methylation and tumorigenesis. *Nature* **539**, 390–395 (2016).
51. C. Priolo *et al*., Tuberous sclerosis complex 2 loss increases lysophosphatidylcholine synthesis in lymphangioleiomyomatosis. *Am. J. Respir. Cell Mol. Biol.* **53**, 33–41 (2015).
52. Y. Zhu *et al*., p21-activated kinase 1 determines stem-like phenotype and sunitinib resistance via NF-κB/IL-6 activation in renal cell carcinoma. *Cell Death Dis.* **6**, e1637 (2015).
53. T. Cuadros *et al*., HAVCR/KIM-1 activates the IL-6/STAT-3 pathway in clear cell renal cell carcinoma and determines tumor progression and patient outcome. *Cancer Res.* **74**, 1416–1428 (2014).
54. C. Garbers, S. Heink, T. Korn, S. Rose-John, Interleukin-6: Designing specific therapeutics for a complex cytokine. *Nat. Rev. Drug Discov.* **17**, 395–412 (2018).
55. T. Tanaka, T. Kishimoto, The biology and medical implications of interleukin-6. *Cancer Immunol. Res.* **2**, 288–294 (2014).
56. H. J. Liu, V. P. Krymskaya, E. P. Henske, Immunotherapy for lymphangioleiomyomatosis and tuberous sclerosis: Progress and future directions. *Chest* **156**, 1062–1067 (2019).
57. S. Koyama *et al*., STK11/LKB1 deficiency promotes neutrophil recruitment and proinflammatory cytokine production to suppress T-cell activity in the lung tumor microenvironment. *Cancer Res.* **76**, 999–1008 (2016).
58. J. Ma *et al*., Mammalian target of rapamycin regulates murine and human cell differentiation through STAT3/p63/Jagged/Notch cascade. *J. Clin. Invest.* **120**, 103–114 (2010).
59. Y. Cui *et al*., Aberrant SYK kinase signaling is essential for tumorigenesis induced by TSC2 inactivation. *Cancer Res.* **77**, 1492–1502 (2017).
60. K. Yokogami, S. Wakisaka, J. Avruch, S. A. Reeves, Serine phosphorylation and maximal activation of STAT3 during CNTF signaling is mediated by the rapamycin target mTOR. *Curr. Biol.* **10**, 47–50 (2000).
61. E. Rad, K. Dodd, L. Thomas, M. Upadhyaya, A. Tee, STAT3 and HIF1α signaling drives oncogenic cellular phenotypes in malignant peripheral nerve sheath tumors. *Mol. Cancer Res.* **13**, 1149–1160 (2015).
62. J. Ye *et al*., Pyruvate kinase M2 promotes de novo serine synthesis to sustain mTORC1 activity and cell proliferation. *Proc. Natl. Acad. Sci. U.S.A.* **109**, 6904–6909 (2012).
63. K. Taniguchi *et al*., A gp130-Src-YAP module links inflammation to epithelial regeneration. *Nature* **519**, 57–62 (2015).
64. K. Taniguchi *et al*., YAP-IL-6ST autoregulatory loop activated on APC loss controls colonic tumorigenesis. *Proc. Natl. Acad. Sci. U.S.A.* **114**, 1643–1648 (2017).
65. W. J. Azar *et al*., Noncanonical IL6 signaling-mediated activation of YAP regulates cell migration and invasion in ovarian clear cell cancer. *Cancer Res.* **80**, 4960–4971 (2020).
66. C. J. Wruck *et al*., Nrf2 induces interleukin-6 (IL-6) expression via an antioxidant response element within the IL-6 promoter. *J. Biol. Chem.* **286**, 4493–4499 (2011).
67. M. Zarei *et al*., Tumors with TSC mutations are sensitive to CDK7 inhibition through NRF2 and glutathione depletion. *J. Exp. Med.* **216**, 2635–2652 (2019).
68. G. M. DeNicola *et al*., NRF2 regulates serine biosynthesis in non-small cell lung cancer. *Nat. Genet.* **47**, 1475–1481 (2015).
69. N. Liang, M. Pende, YAP enters the mTOR pathway to promote tuberous sclerosis complex. *Mol. Cell. Oncol.* **2**, e998100 (2015).
70. C. S. Yang *et al*., Glutamine-utilizing transaminases are a metabolic vulnerability of TAZ/YAP-activated cancer cells. *EMBO Rep.* **19**, e43577 (2018).
71. B. Ngo *et al*., Limited environmental serine and glycine confer brain metastasis sensitivity to PHGDH inhibition. *Cancer Discov.* **10**, 1352–1373 (2020).
72. O. D. Maddocks *et al*., Serine starvation induces stress and p53-dependent metabolic remodelling in cancer cells. *Nature* **493**, 542–546 (2013).
73. S. C. Baksh *et al*., Extracellular serine controls epidermal stem cell fate and tumour initiation. *Nat. Cell Biol.* **22**, 779–790 (2020).
74. J. Yu, A. Astrinidis, E. P. Henske, Chromosome 16 loss of heterozygosity in tuberous sclerosis and sporadic lymphangiomyomatosis. *Am. J. Respir. Crit. Care Med.* **164**, 1537–1540 (2001).
75. J. Yu, A. Astrinidis, S. Howard, E. P. Henske, Estradiol and tamoxifen stimulate LAM-associated angiomyolipoma cell growth and activate both genomic and nongenomic signaling pathways. *Am. J. Physiol. Lung Cell. Mol. Physiol.* **286**, L694–L700 (2004).
76. K. Pollizzi, I. Malinowska-Kolodziej, M. Stumm, H. Lane, D. Kwiatkowski, Equivalent benefit of mTORC1 blockade and combined PI3K-mTOR blockade in a mouse model of tuberous sclerosis. *Mol. Cancer* **8**, 38 (2009).